



Nonlocal damage propagation in the dynamics of masonry elements



Jessica Toti^a, Vincenzo Gattulli^{a,*}, Elio Sacco^b

^a Department of Civil, Construction-Architectural and Environmental Engineering, University of L'Aquila, Italy

^b Department of Civil and Mechanical Engineering, University of Cassino and Southern Lazio, Italy

ARTICLE INFO

Article history:

Received 24 February 2014

Accepted 10 January 2015

Available online 14 March 2015

Keywords:

Dynamic analysis

Masonry

Nonlocal damage

Finite element method

ABSTRACT

In this work, a nonlocal damage-plasticity model for dynamic finite element analyses of cohesive structural elements is presented. The proposed cohesive model is able to reproduce the main relevant behaviors of quasi-brittle materials despite being quite simple, i.e. governed by only a few parameters which can be determined by standard laboratory tests. In particular, the model is able to reproduce the mechanisms of cohesive materials under static or dynamic loads: degradation of the mechanical properties (damage) and accumulation of irreversible strains (plasticity). Moreover, the model also simulates the cyclic macroscopic behavior of quasi-brittle materials, taking into account the loss and recovery of stiffness due to crack closure and reopening. The latter effect represents a particularly important characteristic in the case of dynamic loads. The proposed formulation is implemented as a constitutive model for two-dimensional plane stress four-node quadrilateral elements. The second order equations of motion are solved adopting the implicit Newmark time integration scheme. The proposed model is validated and its dynamic performance is numerically demonstrated through the analysis of a large-scale structural element.

© 2015 Elsevier Ltd. All rights reserved.

1. Introduction

Earthquakes represent one of the major threats to the world's architectural heritage, which consists mostly of structures made of cohesive materials, such as concrete or masonry. Thus, the inelastic dynamic analysis has become an important task for evaluating the safety of existing structures subject to seismic actions. One of the most crucial point in the modeling process is the adoption of appropriate material constitutive laws. Many mathematical models and computational tools have been proposed to date for nonlinear analysis of structures made of cohesive material. Common models able to satisfactory reproduce the cyclic behavior, which is a quite complex phenomenon of cohesive materials, are based on damage mechanics, plasticity theory or a combination of both.

The failure of cohesive material is modeled by constitutive laws characterized by strain softening; indeed, numerical approaches based on standard local constitutive models are widely deemed inappropriate for studying this class of materials. Applications of these models in finite element programs to perform structural

analyses run into severe difficulties. In fact, in a finite element approach, the strain may localize into narrow bands whose width depends on the finite element size and tends to zero when the mesh is refined; consequently, the bulk energy dissipated in the process zone tends to zero. Therefore, the numerical solution becomes ineffective as strongly depending on the choice of mesh made by the analyst. A general and effective way to avoid strain localization into a zero volume and to overcome spurious mesh sensitivity is the use of regularized models based on nonlocal continuum approaches [1–4].

The presence of damage or of other inelastic phenomena modifies the overall structural dynamic response, and the damage propagation potentially interacts dynamically with the element vibrations; in other words, the degradation of the mechanical properties of a system are associated with changes in its structural behavior. Based on these considerations, research efforts have sought to use variations in the dynamic behavior to detect structural damage. Particular attention has been focused on the use of frequencies only, on account of the ease of measuring them and, therefore, their experimental reliability. Within this framework, dynamic analyses of damaged structures have been performed in [5,6] with the aim of detecting damage and evaluating the condition of the structure.

The study of the evolution of damage under dynamic loading has been approached in [7], where a local one-dimensional

* Corresponding author at: Dipartimento Ingegneria Civile, Edile-Architettura, Ambientale, University of L'Aquila, Monteluco di Roio, 67040 L'Aquila, Italy.

E-mail addresses: jessica.toti@unicas.it (J. Toti), vincenzo.gattulli@univaq.it (V. Gattulli), sacco@unicas.it (E. Sacco).

URL: http://dicea.univaq.it/team-view/prof_gattulli/ (V. Gattulli).

constitutive law implemented into a fiber model is proposed for a beam finite element.

In the field of nonlocal constitutive laws, an integral nonlocal damage model is presented in [8], where an explicit time step algorithm is implemented in a parallel finite element code. A gradient nonlocal model for nonlinear dynamic analysis of heterogeneous media is presented in [9], where the coupling between rate-dependent plasticity and rate-independent damage is considered. A nonlinear elasticity approach has been adopted for investigating the transverse vibration of bilayer graphene sheets [10]. Numerical simulations developed adopting both local and nonlocal constitutive laws of high velocity impact problem of a rigid projectile within softening material are presented in [11]; it is shown that the nonlocal model allows to alleviate numerical instabilities, spurious post-bifurcation and mesh dependency solutions.

A further aspect of the dynamics of structures in which evolving damage occurs is the opening and closure of microcracks, which define the damage state. Indeed, when the material is subjected to compressive strain, the microcracks reclose, inducing a stiffening recovery of the damaged material. The unilateral behavior of damaged materials has been studied mainly in the framework of quasi-static cyclic analyses, as for instance in [12–14]. It can be remarked that the unilateral phenomenon can induce peculiar features in the dynamics of damaged elements [5].

It can be remarked that, while there is a great interest in the response of damaging and damaged structures subjected to seismic actions, there is a quite reduced research activity concerning the dynamic structural response in the framework of nonlocal formulations for damage evolution, allowing softening effect. The main purpose of this paper is to give a contribution in this direction, developing a suitable numerical procedure to study the mechanical behavior of structures made of cohesive materials.

On the base of the above considerations, this work explores the dynamic response of two-dimensional cohesive structural elements taking into account the damage evolution, the presence of inelastic strains, and the unilateral effect due to crack closure within a nonlocal constitutive law. To this end, a nonlocal model [15] is formulated in a dynamic framework for investigating the damaging evolution of vibrating structures. Specifically, a slightly modified version of the model is presented and the validation of the formulated methodology in reproducing the degradation of structures under dynamic cyclic loadings is provided. Moreover, the present work presents a set of applications with the aim to validate the model for the dynamic analyses, by emphasizing the importance of the adoption of a nonlocal constitutive law, able to satisfactorily simulate the hysteretic behavior of a cohesive material. Therefore, the presented model reproduces the typical behavior of quasi-brittle materials, while remaining quite simple; indeed, the model is governed by only a few parameters which can be determined by standard laboratory tests. In particular, through the introduction of only five parameters, the model is able to reproduce the main features characterizing the macroscopic response of the quasi-brittle material under static or dynamic loads: degradation of the mechanical properties in tension and in compression, different strengths and softening responses in tension and in compression, evolution of irreversible strains, and unilateral phenomena due to microcrack reclosure and nonlocal stress-strain relationships. The proposed formulation is implemented as a constitutive model for two-dimensional, four-node quadrilateral elements in a research version of the finite element code FEAP [16,17]. The second-order equations of motion are solved adopting the implicit Newmark time integration scheme.

The dynamic performance of the proposed model is assessed through the numerical analysis of a large-scale structural element. Specifically, a vertical structural member belonging to the Basilica of S. Maria di Collemaggio, an important medieval church located

in L'Aquila town and heavily damaged during the 2009 earthquake, is considered as a case study. The damage propagation induced in the examined mechanical system by two types of imposed base motion, i.e. by a simple harmonic motion and by the motion produced during 2009 L'Aquila earthquake, is investigated. The variations in the dynamic behavior (i.e. displacement amplitudes, frequency contents, hysteretic dissipation energy) due to harmonic motions are analyzed for the structural member with respect to undamaged condition. The performance of the cohesive model in reproducing the degradation state observed after 2009 L'Aquila earthquake are tested. Furthermore, some advantages provided by the nonlocal approach, compared to the local formulation, are verified for both applied loading functions.

The paper is organized as follows. First, the governing equations of the cohesive model are provided. Then, the numerical procedure is briefly presented and the results of some numerical applications are illustrated. Finally, concluding remarks are made.

2. Cohesive constitutive model

2.1. Constitutive law

The following isotropic damage model is introduced:

$$\boldsymbol{\sigma} = \bar{\boldsymbol{\sigma}} [(1 - D_t)H(J_1^e) + (1 - D_c)(1 - H(J_1^c))] \quad (1)$$

where $\boldsymbol{\sigma}$ and $\bar{\boldsymbol{\sigma}}$ are the stress tensor and effective stress tensor, respectively; D_t and D_c are two damage variables which capture the stiffness degradations of the concrete in tension and compression; $J_1^e = \text{tr}(\boldsymbol{\epsilon})$ is the first invariant of the elastic strain; $H(x)$ denotes the Heaviside function (i.e. $H(x) = 1$ if $x \geq 0$, otherwise $H(x) = 0$). In formula (1), as the damage variables affect the whole effective stress $\bar{\boldsymbol{\sigma}}$, an isotropic damage state is implicitly considered.

The effective stress tensor is computed as:

$$\bar{\boldsymbol{\sigma}} = \mathbf{C} : (\boldsymbol{\epsilon} - \boldsymbol{\pi}) = \mathbf{C} : \mathbf{e} \quad (2)$$

where $\boldsymbol{\epsilon}$, $\boldsymbol{\pi}$ and \mathbf{e} are the total strain, the plastic strain and the elastic strain, respectively; \mathbf{C} is the fourth-order elastic stiffness tensor; the colon symbol indicates the double contraction.

It can be remarked that the constitutive law defined by Eqs. (1) and (2) leads to discontinuities in the stress-strain relationship. Indeed, considering an isotropic cohesive material subjected to a shear strain γ_{12} accompanied with $\epsilon_{11} = \epsilon_{22} = \alpha$, the shear stress is $\tau_{12} = G\gamma_{12}[(1 - D_t)H(\alpha) + (1 - D_c)(1 - H(\alpha))]$, with G the shear modulus. Setting $D_t > D_c$ and taking γ_{12} as a constant, τ_{12} suddenly modifies when the value of α changes from negative to positive. It can be considered realistic to have a stiffer shear response when the material point is subjected to volumetric contraction ($\alpha < 0$) with respect to the case of volumetric expansion ($\alpha > 0$), because of the positive effect of the friction in compression. However, this strong discontinuity of the response in the material point is undesirable from both a physical and a mathematical point of view. For this reason, in order to avoid the strong discontinuity in the stress value, a regularized form of the Heaviside function is adopted in the present model; in particular, it is posed:

$$H(x) = \frac{1}{1 + e^{-x/h}} \quad (3)$$

where h is a small parameter governing the regularization effect ($h = 0.001\text{--}0.0005$).

The introduction of the regularization function (3) in the constitutive law (1) does not completely overcome the deficiency of the model but improves and confines the sudden jumps, which occur for infrequent cyclic strain paths.

2.2. Evolution law of the plastic strain

The evolution of the plastic strain is described by introducing a yield function, which is a branch of a modified hyperbola (Fig. 1a), the associative law and the loading–unloading conditions in the Kuhn–Tucker form:

$$f_Y(\bar{\boldsymbol{\sigma}}) = A - (\bar{\sigma}_1 - \bar{\sigma}_Y)(\bar{\sigma}_2 - \bar{\sigma}_Y) + B \left[\langle \bar{\sigma}_1 - \bar{\sigma}_Y \rangle_-^2 + \langle \bar{\sigma}_2 - \bar{\sigma}_Y \rangle_-^2 \right] \leq 0 \quad (4)$$

$$\dot{\boldsymbol{\pi}} = \dot{\lambda} \frac{\partial f_Y}{\partial \bar{\boldsymbol{\sigma}}} \quad (5)$$

$$\dot{\lambda} \geq 0, \quad f_Y(\bar{\boldsymbol{\sigma}}) \leq 0, \quad \dot{\lambda} f_Y(\bar{\boldsymbol{\sigma}}) = 0 \quad (6)$$

respectively, where $\bar{\sigma}_1$ and $\bar{\sigma}_2$ are the principal stresses of the effective stress tensor $\bar{\boldsymbol{\sigma}}$; the bracket symbol $\langle \cdot \rangle_-$ denotes the negative part of the number; $\bar{\sigma}_Y$ is the material parameter linked to the uniaxial compressive strength of the concrete σ_Y thorough the expression $\bar{\sigma}_Y = (A + \sigma_Y^2)/\sigma_Y$; A and B are parameters governing the shape of the yield function whose values are assumed in the following analyses as $A = 0.1 \text{ N}^2/\text{mm}^4$ and $B = 1$; $\dot{\lambda}$ is the plastic multiplier.

2.3. Evolution law of the damage

As a damage softening constitutive law is introduced, the localization of the strain and damage could occur. In order to overcome this pathological problem, to account for the correct size of the localization zone and, also, to avoid strong mesh sensitivity in the numerical results in finite element analyses, a nonlocal constitutive law is considered both for the compressive and tensile damage.

In particular, the evolution of the compressive damage D_c is combined with the development of the plastic strain through the following cubic relationship:

$$D_c = \max_{\text{history}} \{ \min \{ 1, \tilde{D}_c \} \} \quad \text{with} \quad \tilde{D}_c = -\frac{2}{\kappa_u^3} \bar{\kappa}^3 + \frac{3}{\kappa_u^2} \bar{\kappa}^2 \quad (7)$$

where κ_u is the final accumulated plastic strain associated with the compressive damage $D_c = 1$; $\bar{\kappa}$ is the nonlocal accumulated plastic strain:

$$\bar{\kappa}(\mathbf{x}) = \frac{1}{\int_{\Omega} \psi_c(\mathbf{x}, \mathbf{y}) d\Omega(\mathbf{y})} \int_{\Omega} \psi_c(\mathbf{x}, \mathbf{y}) \kappa(\mathbf{y}) d\Omega(\mathbf{y}) \quad (8)$$

with κ the local value of the accumulated plastic strain, and ψ_c the weight function in compression which determines the influence of

the point \mathbf{y} on \mathbf{x} ; in particular, the function ψ_c is set to depend only on the distance $\|\mathbf{x} - \mathbf{y}\|$ as:

$$\kappa = \int_0^t \|\dot{\boldsymbol{\pi}}\| dt \quad \psi_c(\mathbf{x}, \mathbf{y}) = \left\langle 1 - \frac{\|\mathbf{x} - \mathbf{y}\|^2}{R_c^2} \right\rangle_+ \quad (9)$$

In Eq. (9), the bracket symbol $\langle \cdot \rangle_+$ denotes the positive part of the number, the parameter $2R_c$ is the characteristic length, determining the size of the volume Ω , which significantly contributes to the definition of the nonlocal accumulated plastic strain.

The evolution of the tensile damage parameter D_t is governed through the following nonlocal exponential law:

$$D_t = \max_{\text{history}} \{ 0, \tilde{D}_t \} \quad \text{with} \quad \tilde{D}_t = \frac{\bar{\varepsilon}_{eq} - \varepsilon_0 \exp(-k(\bar{\varepsilon}_{eq} - \varepsilon_0))}{\bar{\varepsilon}_{eq}} \quad (10)$$

where ε_0 is a material parameter indicating the strain damage threshold; k is a parameter governing the softening branch of the stress–strain relation and is related to the damage tensile fracture energy $G_t = E\varepsilon_0(\varepsilon_0 k + 2)/(2k)$; $\bar{\varepsilon}_{eq}$ is the nonlocal equivalent elastic strain:

$$\bar{\varepsilon}_{eq}(\mathbf{x}) = \frac{1}{\int_{\Omega} \psi_t(\mathbf{x}, \mathbf{y}) d\Omega(\mathbf{y})} \int_{\Omega} \psi_t(\mathbf{x}, \mathbf{y}) \varepsilon_{eq}(\mathbf{y}) d\Omega(\mathbf{y}) \quad (11)$$

with the equivalent elastic strain ε_{eq} and weight function in tension ψ_t , which determines the influence of the point \mathbf{y} on \mathbf{x} , defined as:

$$\varepsilon_{eq} = \sqrt{\langle e_1 \rangle_+^2 + \langle e_2 \rangle_+^2} \quad \psi_t(\mathbf{x}, \mathbf{y}) = \left\langle 1 - \frac{\|\mathbf{x} - \mathbf{y}\|^2}{R_t^2} \right\rangle_+ \quad (12)$$

In Eq. (12), e_1 and e_2 are the principal elastic strains. Moreover, the condition that the damage in compression must not be lower than the one in tension is assumed $D_t \geq D_c$. The graph of the limit function for the tensile damage in principle stresses field is reported in Fig. 1a. A qualitative trend of the local responses of the cohesive model in tension and in compression is shown in Fig. 1b.

3. Motion equations and finite element discretization

A deformable body Ω subjected to a motion is considered; the weak form of the linear momentum balance, or virtual work expression, takes the following form:

$$\int_{\Omega} \boldsymbol{\sigma} : \delta \boldsymbol{\varepsilon} d\Omega + \int_{\Omega} \rho \mathbf{a} \cdot \delta \mathbf{u} d\Omega - \int_{\Omega} \mathbf{b} \cdot \delta \mathbf{u} d\Omega - \int_{\partial\Omega} \mathbf{t} \cdot \delta \mathbf{u} d\Omega = 0 \quad (13)$$

where ρ is the mass density, \mathbf{a} is the acceleration, \mathbf{b} is the body force, \mathbf{t} is the traction force acting on $\partial\Omega$, $\delta \boldsymbol{\varepsilon}$ is a strain field compatible with the admissible displacement field $\delta \mathbf{u}$.

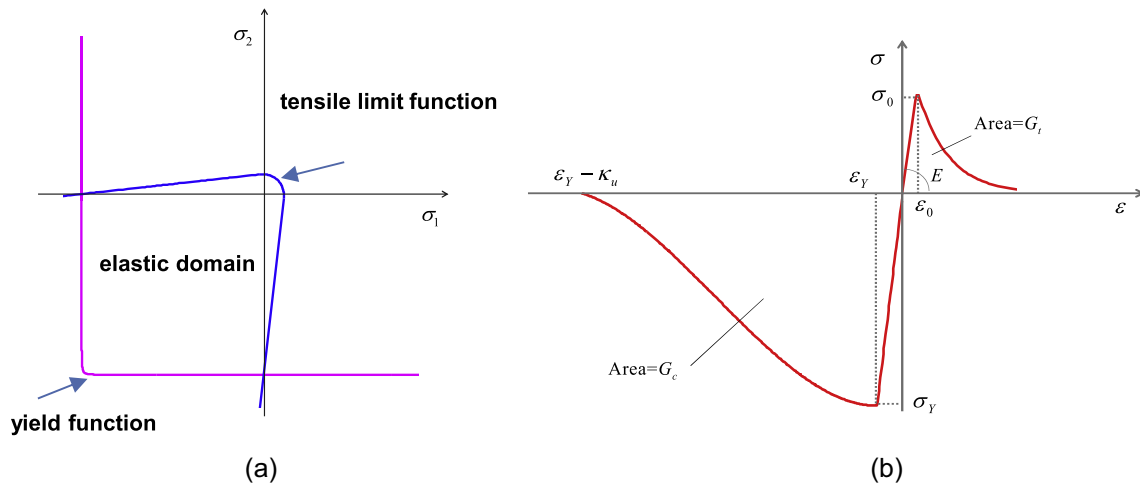


Fig. 1. (a) Elastic domain in the principal stress space; (b) Uniaxial response in tension and compression.

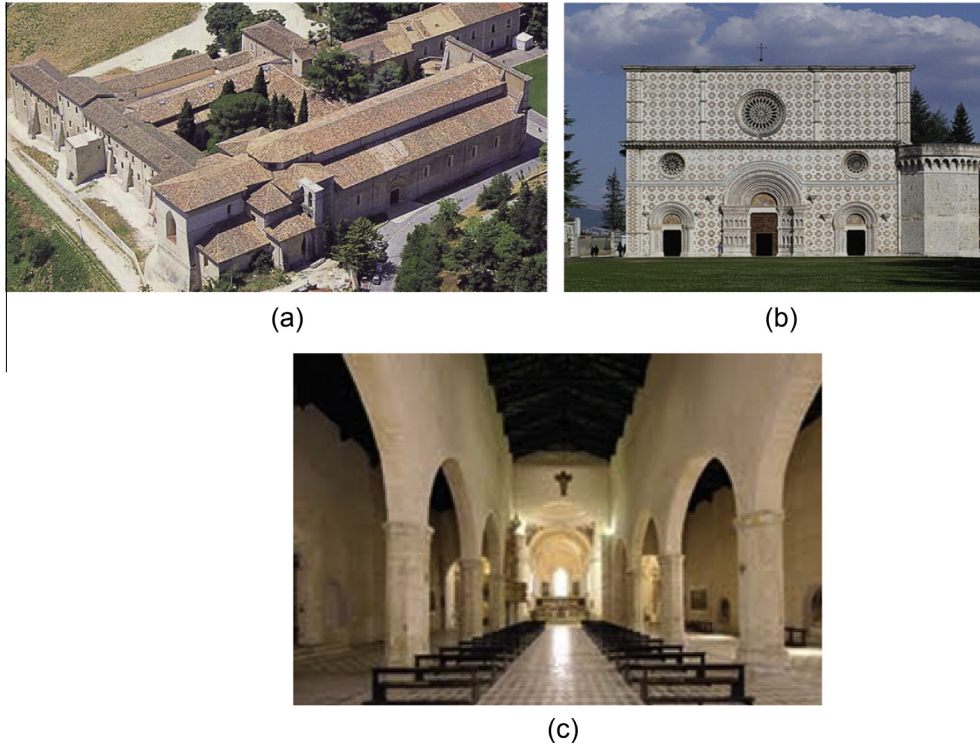


Fig. 2. Basilica S. Maria di Collemaggio: (a) view of entire historical complex; (b) facade; (c) naves.

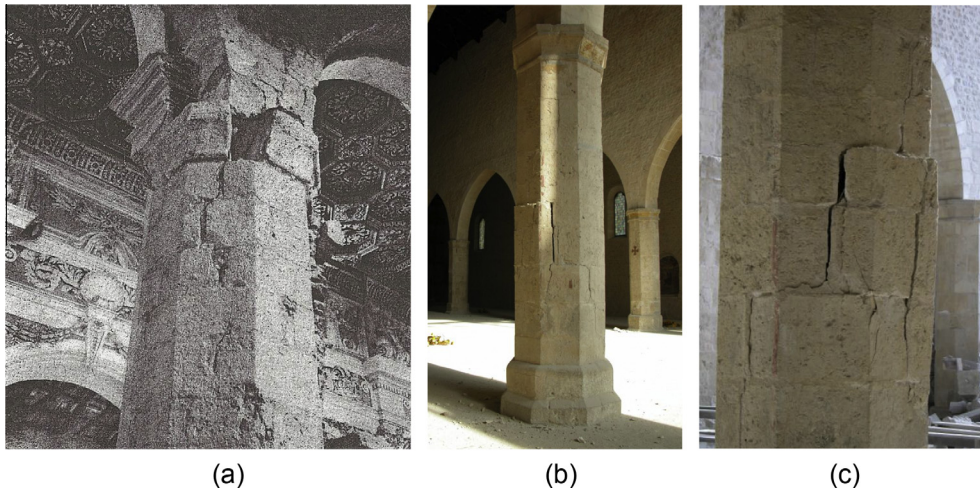


Fig. 3. Cracking in the octagonal central column located in the hall due to out-of-plane-mechanism caused by earthquakes; (a) found during the restoration of the 1970s; (b, c) after the 2009 L'Aquila earthquake.

The body Ω is discretized into finite elements Ω_e and a suitable displacement interpolation is introduced into the virtual displacement expression, which leads to the ordinary differential system of equations of motion:

$$\mathbf{M}\ddot{\mathbf{u}} + \mathbf{f}^{\text{int}}(\mathbf{u}) = \mathbf{f}^{\text{ext}} \quad (14)$$

where \mathbf{u} is the nodal displacement vector and $\ddot{\mathbf{u}}$ the nodal acceleration vector, in which dots denote the derivative with respect to time. In Eq. (14) the mass matrix \mathbf{M} , the internal forces vector \mathbf{f}^{int} , and the external force acting upon the system \mathbf{f}^{ext} are obtained assembling the element mass matrix and force vectors:

$$\begin{aligned} \mathbf{M}_e &= \int_{\Omega_e} \rho \mathbf{N}^T \mathbf{N} d\Omega \\ \mathbf{f}_e^{\text{int}} &= \int_{\Omega_e} \mathbf{B}^T \boldsymbol{\sigma} d\Omega \\ \mathbf{f}_e^{\text{ext}} &= \int_{\Omega_e} \mathbf{N}^T \mathbf{b} d\Omega + \int_{\partial\Omega_e} \mathbf{N}^T \mathbf{t} d\Omega \end{aligned} \quad (15)$$

The matrices \mathbf{N} and \mathbf{B} contain the conventional element interpolation functions and its derivatives, respectively. Notice that in the second expression of the Eq. (15), the stress tensor $\boldsymbol{\sigma}$ is a function of the damage variables governed by nonlocal measure of the strain scalar quantities, $\bar{\kappa}$ and $\bar{\varepsilon}_{eq}$, defined in the relationships (8) and (11).

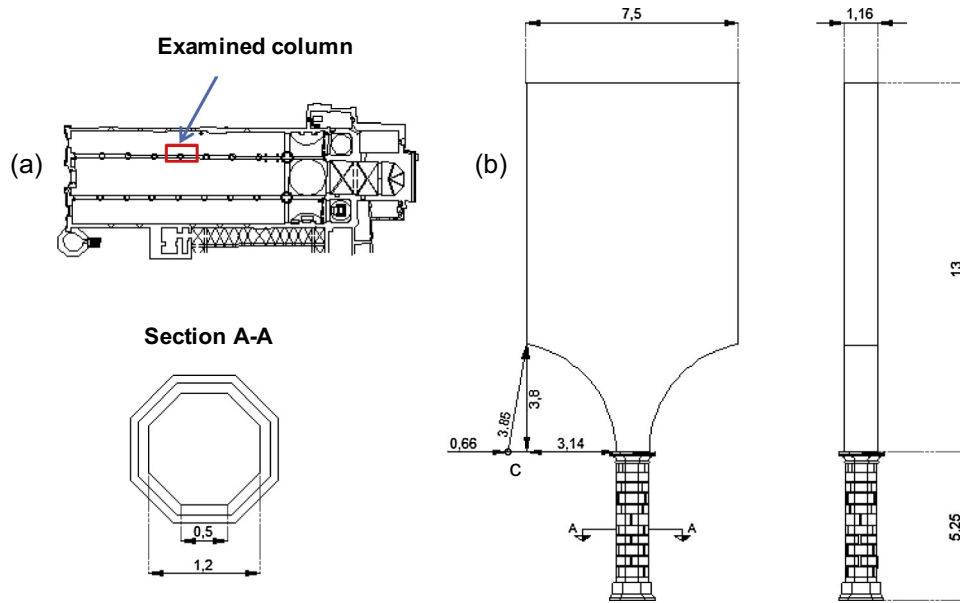


Fig. 4. Examined structural system: (a) position in plan; (b) geometry (units in meters).

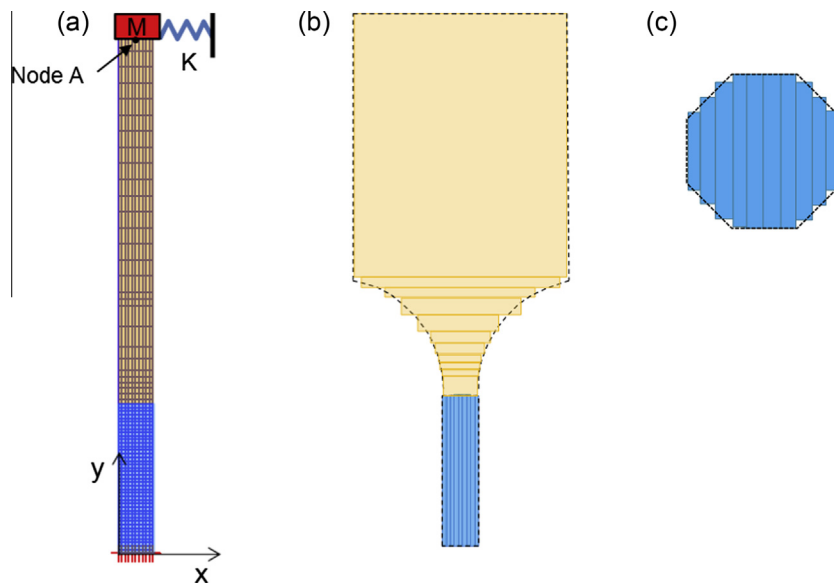


Fig. 5. Finite element modeling of the examined structural system: (a) discretization and initial boundary condition; (b) modeling of the geometry of the ogival arch; (c) modeling of the cross section of the octagonal pillar.

Table 1
Material parameters.

	E (N/mm ²)	ν	ϵ_0	σ_Y (N/mm ²)	κ_u	G_r (N/mm ²)	R (m)	ρ (kN/m ³)
Ogival arch	2500	0.2	0.00012	-3	0.07	0.01	0.4	21.35
Column	20400	0.2	0.00005	-3	0.07	0.01	0.4	17

From the set of Eq. (14), only the equations related to the free-coordinates $\tilde{\mathbf{u}}$ can be discerned and, taking into account the boundary conditions on the restrained-coordinates $\hat{\mathbf{u}}$, they are rewritten in following form:

$$\tilde{\mathbf{M}}\ddot{\tilde{\mathbf{u}}} + \tilde{\mathbf{f}}^{\text{int}}(\tilde{\mathbf{u}}) = \tilde{\mathbf{f}}^{\text{ext}} - \tilde{\mathbf{M}}\mathbf{r}\ddot{u}_g \quad (16)$$

where $\tilde{\mathbf{M}}$, $\tilde{\mathbf{f}}^{\text{int}}$ and $\tilde{\mathbf{f}}^{\text{ext}}$ are the restrictions of \mathbf{M} , \mathbf{f}^{int} and \mathbf{f}^{ext} to the degrees of freedom $\tilde{\mathbf{u}}$; moreover, u_g is an imposed displacement

time-history at the ground in the direction described by the allocation vector \mathbf{r} , and \ddot{u}_g is its second time derivative, i.e. the ground acceleration.

The proposed nonlocal material model is implemented as a constitutive model for two-dimensional four-node quadrilateral elements in a research version of the finite element code FEAP [17]. In the implementations, the integrals of Eq. (15) are solved adopting the Gauss–Legendre quadrature technique. The second order

equations of motion (16) are solved adopting the implicit Newmark time integration scheme setting $\delta = 1/2$ and $\alpha = 1/4$.

4. Damage propagation in a large-scale structural system

4.1. Case study

The damage propagation in a large-scale structure under in-plane loading is investigated. In particular, the study analyzes the local dynamic behavior of a particular structural member belonging to the Basilica S. Maria di Collemaggio, the most celebrated medieval church in the Italian Region of Abruzzo, located in the town of L'Aquila. The architectonic complex of S. Maria di Collemaggio comprises the church and the monastery (Fig. 2a).

The church is famous for the elegant Romanesque facade (Fig. 2b), which features a central door and two smaller flanking doors; each door is a round arch set into a series of archivolt, and each is surmounted by a rose window. The main decoration of the facade consists in contrasting stone arranged in a sort of tapestry of cruciform elements. An octagonal belfry located on the left side of the facade gives the building an asymmetrical appearance. The interior hall follows the standard plan of a nave and two side aisles. Each side aisle is divided from the nave by a row of seven columns (Fig. 2c), from which ogival arches support a tall wooden ceiling (Fig. 2c). The hall is separated from the transept by two large columns, which support the two barrel vaults, the dome and a part of the internal walls. The transept of the Basilica does not produce the so called “Latina cross shape” because it does not extend beyond the perimeter wall of the side aisles. Finally, behind the transept there are a presbytery and three apses constructed in masonry.

Over the years, the basilica has undergone numerous transformations, whether due to earthquake damages or stylistic renovation. In the last thirty years, numerous research experiments and numerical studies have been undertaken with the purpose of understanding the dynamic behavior of this historical monument, e.g. [18,19]. Several diagnostic tests and renovations have been carried out in order to improve the static and dynamic behavior of the basilica.

The most recent works were performed on the basilica immediately after the devastating earthquake, of 5.8 Richter magnitude, which struck L'Aquila on the 6th of April, 2009. The main shock caused the collapse of the dome and the large pillars beneath it, as well as severe damage to the presbytery and almost all of the columns in the hall. In particular, the structural interventions performed on the monument to preserve it during aftershocks and up to reconstruction included: the positioning of a temporary roof in the transept area, the strengthening of the ends of the two internal masonry walls by the use of fiber reinforced polymer (FRP) strips, the shoring up of the internal walls localized in the hall, the wrapping of all columns with polyester belts, the installation of steel ties connecting the side panels, the restoration of the façade, and the installation of a permanent structural monitoring system [20,21].

The Basilica presents a slender shape in the direction parallel to the naves, and the absence of significant transversal walls makes the panels of the hall seismically vulnerable for out-of-plane actions. For this reason, the strong earthquakes which have occurred in the territory of L'Aquila in recent years have often caused severe damage to the columns in the hall, which damage has been characterized by large and deep corresponding cracks in the bases and tops of the columns, mainly due to out-of-plane mechanisms (Fig. 3).

In view of the above, the numerical analyses developed here have the purpose of examining the vibrations and the degradation of a single hall pillar under different out-of-plane loadings. In

particular, the central pillar belonging to the left internal wall is considered; this central pillar is the one farthest from the two transversal walls and, as a consequence, it is the least constrained, subject to higher stresses, and the most free to deform.

The geometry of the studied structural system is depicted in Fig. 4. It is composed of the central stone column and two half ogival arches above it, which belong to the influence area of the pillar. The stone column is 5.25 m high with an octagonal cross section, each of the eight sides measuring 0.5 m wide, and the column as a whole measuring 1.2 m wide. The masonry arch has a thickness of 1.16 m and extends to a height of 13 m from the top of the pillar to the high wooden ceiling; the distance between the two consecutive keystones is 7.5 m. The ogival arch is characterized by a mid-span, a rise, and a radius which measure 3.14, 3.8 and 3.85 m, respectively; the centers of the two circumferences constituting it are shifted 0.66 m with respect to the midspan.

4.2. Modeling

The large scale structural member is modeled using the developed two-dimensional four-node quadrilateral element, where the isotropic damage model is implemented at Gauss point level. It has to underline that the adoption of the isotropic damage model for the macromechanical analysis of the masonry structures is an approximation and the use of an orthotropic model would be more appropriate. The use of an isotropic damage model is often not strongly limiting, as the geometric distribution of the damage field leads to the formation of specific areas highly damaged, which are responsible for the collapse mechanisms governing the response of the structure.

The discretization of the structural system is characterized by a total of 700 finite elements. This choice of mesh assures a satisfactory numerical result, particularly with reference to the initial evaluation of the elastic modal analysis. Indeed, considering refined meshes characterized by a number of finite elements greater than 700, the first fundamental modal frequencies and shapes do not change. The finite element discretization of the two-dimensional model is schematically illustrated in Fig. 5. In particular, the adopted mesh is depicted in Fig. 5a, while Fig. 5b and c show the strategy in modeling the ogival arch and column geometry, respectively. Specifically, the geometry of the arch and the octagonal cross section of the pillar are modeled by modulating the thickness of the two-dimensional finite elements.

The adopted mechanical properties for the stone pillar and the masonry ogival arch are reported in Table 1, where they it is set $R_c = R_t = R$. The material parameters are selected by local tests [20] on undamaged masonry samples. In particular, the elastic properties (E, ν) of the materials are defined through the results of ultrasonic testing, while the post peak parameters in tension (ε_0, G_t) and in compression (σ_Y, κ_u) are determined on the base of single and double flat-jack tests. The dimension of the parameter R has been set in function of the maximum heterogeneity size, which is linked to the size of the clay brick presented in the masonry.

In order to take into account the influence of the connection of the selected portion of the nave with the remaining structure and

Table 2
Comparison of the natural frequencies of the two different models.

Mode	\hat{f} [Hz]	f [Hz]	Error [%]
1	1.449	1.455	0.41
2	4.531	4.593	1.37
3	9.073	9.331	2.76
4	20.964	21.875	4.16

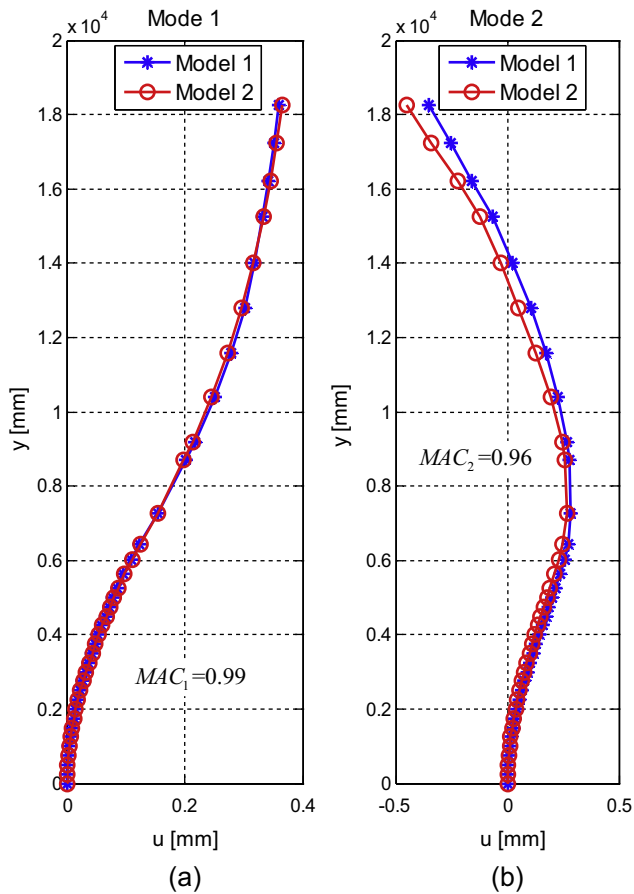


Fig. 6. Comparison between the axis pillar modal shapes obtained considering the two different models: (a) Mode 1; (b) Mode 2.

with the roof, concentrated masses and springs acting in a horizontal direction are considered in the upper nodes of the finite element model. The applied masses and the stiffness of the springs are indicated with M and K , respectively. As an *a priori* evaluation of these two parameters could be quite cumbersome, an inverse procedure based on error minimization is adopted here.

Furthermore, as the examined zone is located very far from the two transversal walls, the masonry panel contiguous to the examined structural system does not provide significant stiffness to the out-of-plane oscillations. For this reason, their eventual contributions are only modeled by the springs at the top without considering other elastic connections along the wall of the ogival arch. The above observation is also confirmed in a study recently carried out by Gattulli et al. [20], in which a refined finite element model of the basilica is developed in order to understand the dynamic behavior evidenced during the 2009 L'Aquila earthquake. In that work, a linear modal analysis of the entire church has been provided and, from the results of the natural shapes, it appears evident that the whole central zone of the masonry walls located in the hall, including the examined central pillar, in correspondence with the bending out-of-plane modes, oscillates transversally with the remaining part of the structure furnishing only a global stiffness and mass participation.

4.3. M and K parameter setting

The setting of the parameters M and K is performed assuring that the dynamic characteristics, computed in terms of the natural frequencies and modes of the two-dimensional model herein developed, are equal to those ones obtained by the finite element

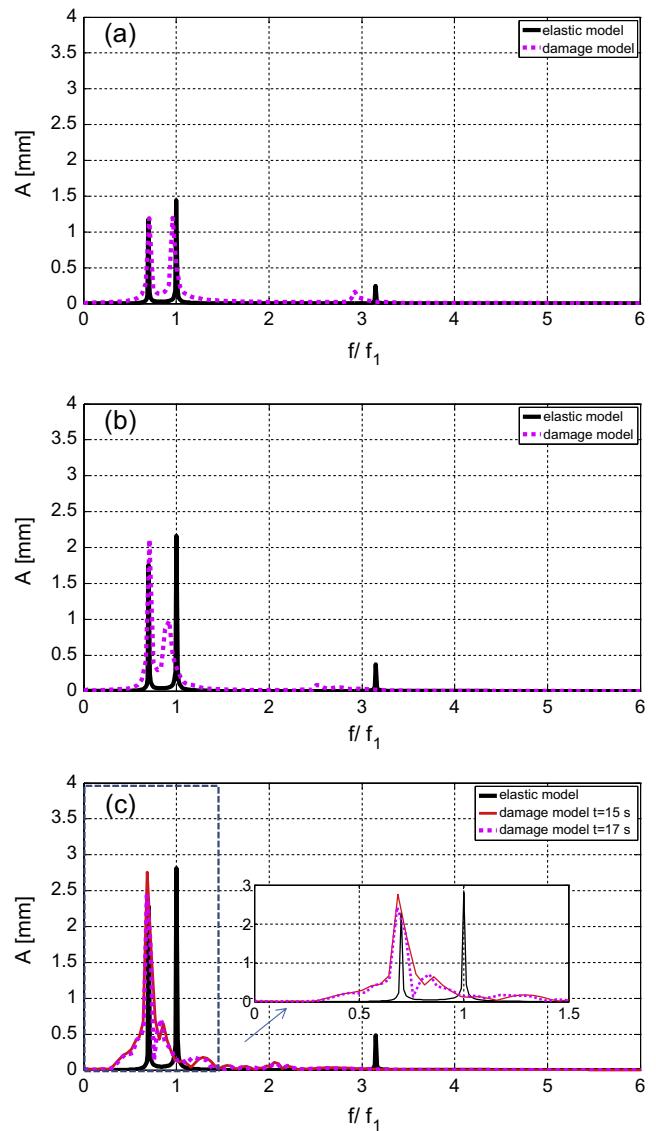


Fig. 7. Fourier spectra of the displacement response: $\eta = 0.7$, (a) $u_0 = 2$ mm, (b) $u_0 = 3$ mm, (c) $u_0 = 4$ mm.

modeling of the entire basilica. In particular, the dynamic parameters of the whole church, as previously mentioned, are reported in [21].

Specifically, the modal parameters related to the first two modes of vibration are considered. The first two out-of-plane frequencies and flexional modal shapes, determined through a linear dynamic analysis of the entire basilica, are denoted, respectively, as $\hat{f}_1, \hat{\psi}_1$ and $\hat{f}_2, \hat{\psi}_2$.

It has to be emphasized that the two vectors $\hat{\psi}_1$ and $\hat{\psi}_2$, although provided by modal analysis of the modeling of the entire structure, are a reduced portion of the complete modal vectors, and have been extracted considering only the horizontal and vertical displacement components u, v belonging to the symmetry axis of the analyzed structural system.

It can be remarked that the numerical solution of the eigenvalue problem, derived from the two-dimensional modeling of the considered substructure, heavily depends on the values of the two parameters M and K . Indeed, the first two frequencies and modal shapes are denoted as $f_1(M, K), \psi_1(M, K)$ and $f_2(M, K), \psi_2(M, K)$, respectively.

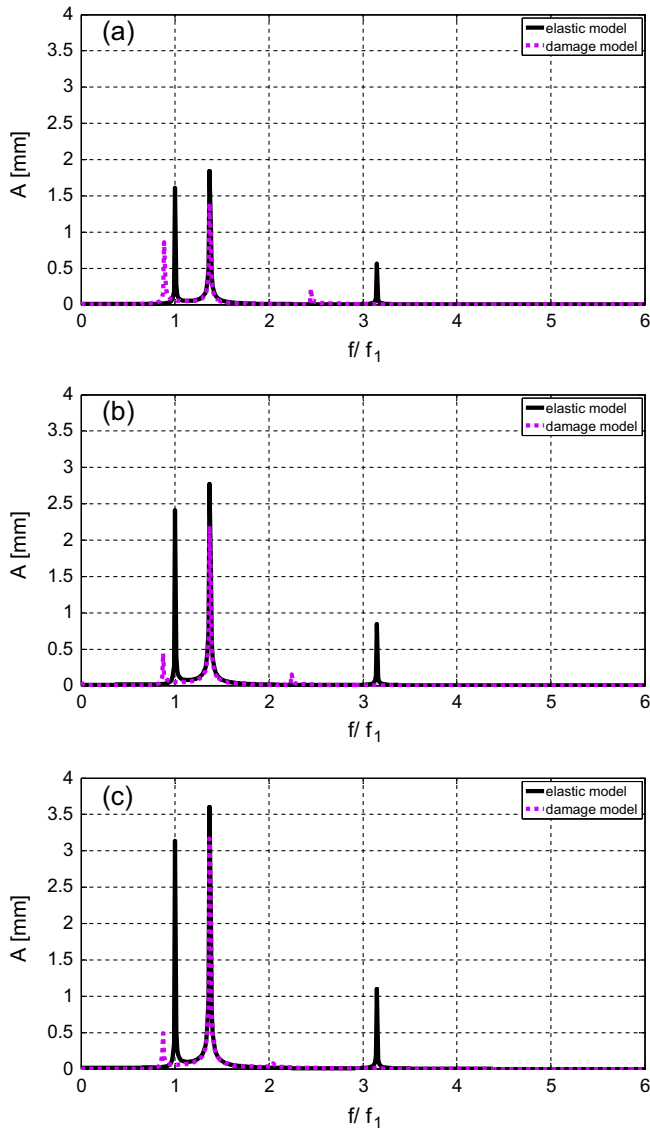


Fig. 8. Fourier spectra of the displacement response: $\eta = 1.3$, (a) $u_0 = 2$ mm, (b) $u_0 = 3$ mm, (c) $u_0 = 4$ mm.

Also in this case the vectors ψ_1 and ψ_2 contain only the components of nodal displacement belonging to the axis of the two-dimensional structural system. Therefore, $\widehat{\psi}_1, \widehat{\psi}_2$ and ψ_1, ψ_2 are the subeigenvectors deriving from two different models and represent

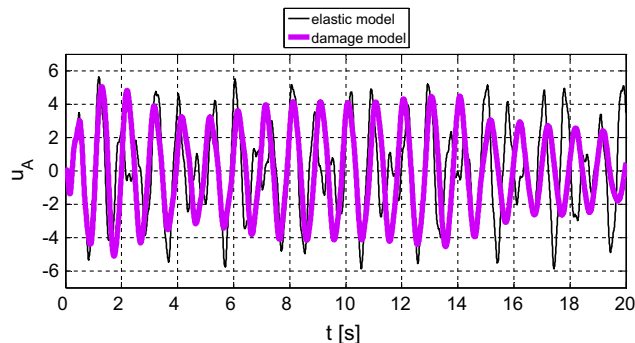


Fig. 9. Time history of the control displacement u_A for $\eta = 0.7$ and $u_0 = 4$ mm.

the modal shapes of the axis of the studied structural system. They have the same size because the two-dimensional model herein developed adopts a finite element discretization so that the same nodes are introduced along the axis of the structural system as in the model proposed in [21].

The following four equivalence conditions between the dynamic characteristics of the two different models are enforced:

$$\frac{f_i}{\widehat{f}_i} = 1$$

$$MAC_i = MAC(\psi_i, \widehat{\psi}_i) = \frac{|\psi_i^T \widehat{\psi}_i|^2}{\psi_i^T \psi_i \widehat{\psi}_i^T \widehat{\psi}_i} = 1 \quad \text{with } i = 1, 2 \quad (17)$$

where the acronym MAC stands for Modal Assurance Criterion. In the equivalence relationships (17), the first two expressions assure the equality between the corresponding frequencies, while the last two equations guarantee the correlation between the two mode shapes, ψ_i and $\widehat{\psi}_i$ with $i = 1, 2$. In particular, for quantifying the comparison of the pair of eigenvectors ψ_1, ψ_2 and $\widehat{\psi}_1, \widehat{\psi}_2$, the Modal Assurance Criterion yields a good statistical indicator and a degree of consistency between mode shapes [22]. It is easy to apply and does not require an estimate of the mass matrix. It is bounded between 0 and 1, with 1 indicating fully consistent mode shapes, while a value of the MAC near to 0 indicating that the modes are not consistent. Therefore, it can only indicate consistency and does not assure orthogonality, which in distinction from the case of model updating [23], is not here required.

The mass M and the spring K values, which approximately satisfy the equivalence conditions (17), are adopted. In order to find these parameters, the Eq. (17) are rewritten in residual form:

$$R_i = (f_i/\widehat{f}_i - 1)$$

$$R_{i+2} = (MAC_i - 1) \quad \text{with } i = 1, 2 \quad (18)$$

and accordingly, the residual function is defined as follows $f_R = \|\mathbf{R}\|$. Indeed, the approximate solution of the problem (17) is determined finding the values M and K which minimize the function f_R . Specifically, the solution is found using an optimization function in MATLAB [24], which leads to have the following approximate solution $M = 5.2[\text{Ns}^2/\text{mm}]$ and $K = 6690[\text{N}/\text{mm}]$.

The comparison between the natural frequencies and shapes provided by the two types of analysis are shown in Table 2 and Fig. 6, respectively. In Fig. 6, the numerical result obtained by considering the global model of the basilica is indicated with Model 1, while the one deriving from the partial model is named Model 2. Finally, from Table 2 and Fig. 6 it is possible to observe that the selected mass and spring values lead to a very satisfactory accordance between the modal parameters linked to the first two modes of vibrations. Moreover, from Table 2 it is evident that the provided identification procedure leads to reasonable results also for the third and fourth modes.

4.4. Harmonic loading

Numerical analyses are conducted to investigate the damage propagation induced by a sinusoidal synchronous motion applied to all nodes of base:

$$u_g(t) = u_0 \sin(2\pi f_0 t) \quad (19)$$

where f_0 and u_0 indicate the frequency and the displacement amplitude of the harmonic imposed displacement, respectively.

The structural response is analyzed for different values of the frequency ratio $\eta = f_0/f_1$; specifically, in the numerical simulations are considered two different values: $\eta = 0.7$ and $\eta = 1.3$. For each

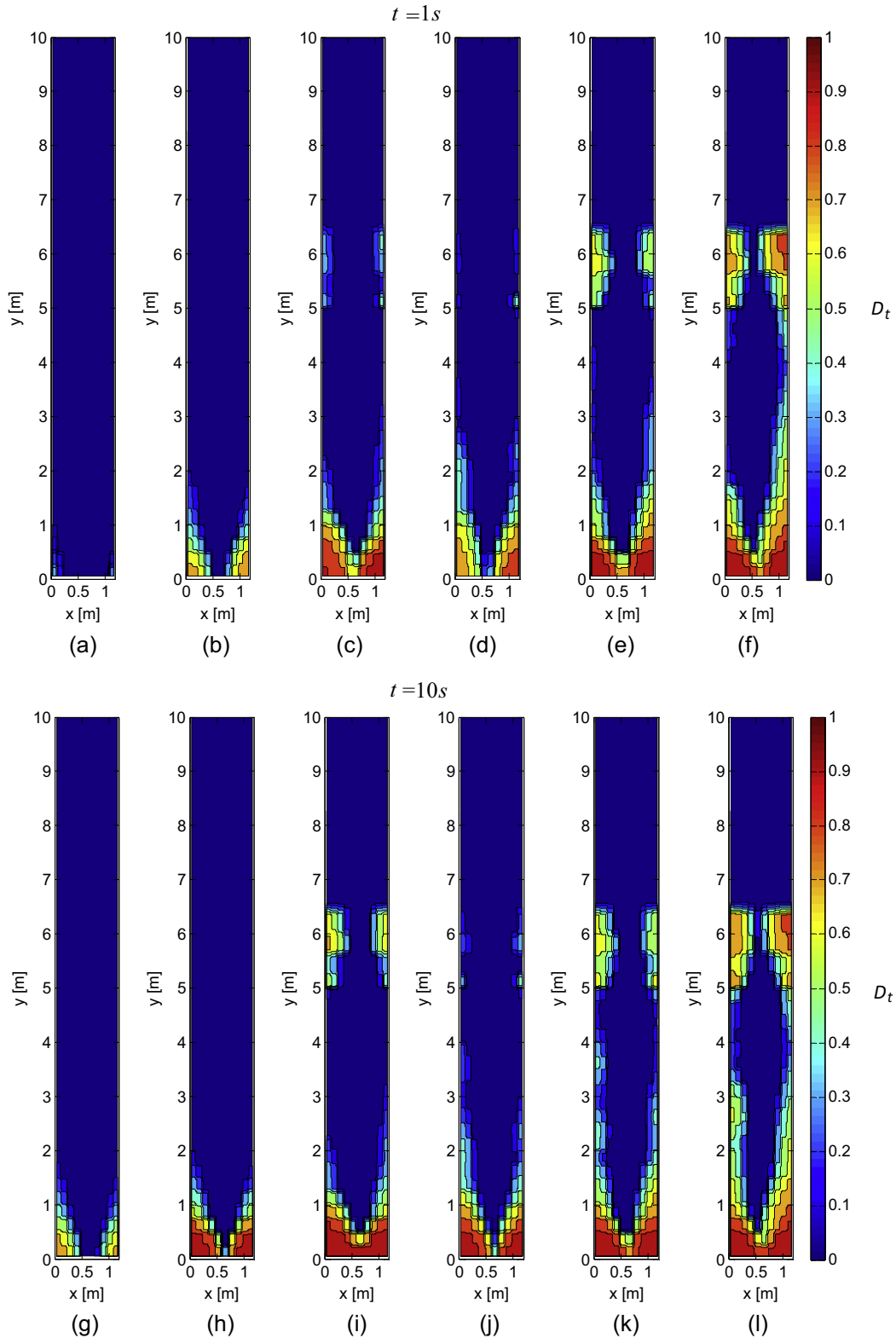


Fig. 10. Damage maps at time step $t = 1$ s with (a) $\eta = 0.7, u_0 = 2$ mm, (b) $\eta = 0.7, u_0 = 3$ mm, (c) $\eta = 0.7, u_0 = 4$ mm; (d) $\eta = 1.3, u_0 = 2$ mm, (e) $\eta = 1.3, u_0 = 3$ mm, (f) $\eta = 1.3, u_0 = 4$ mm and $t = 10$ s with (g) $\eta = 0.7, u_0 = 2$ mm, (h) $\eta = 0.7, u_0 = 3$ mm, (i) $\eta = 0.7, u_0 = 4$ mm; (l) $\eta = 1.3, u_0 = 2$ mm, (m) $\eta = 1.3, u_0 = 3$ mm, (n) $\eta = 1.3, u_0 = 4$ mm.

frequency ratio, the response of the structural system is evaluated for increasing values of the amplitude of the base motion: $u_0 = 2$ mm, $u_0 = 3$ mm and $u_0 = 4$ mm.

The equations of motion are integrated until the final time $t_f = 60$ s, with a time step equal to $\Delta t = 0.005$ s, which

corresponds approximately to 1/40 of the second natural period of vibration.

The response comparisons between the damage and the elastic models are provided in terms of time histories of the displacement u_A of the center point at the top of the structure (Fig. 5). The effect

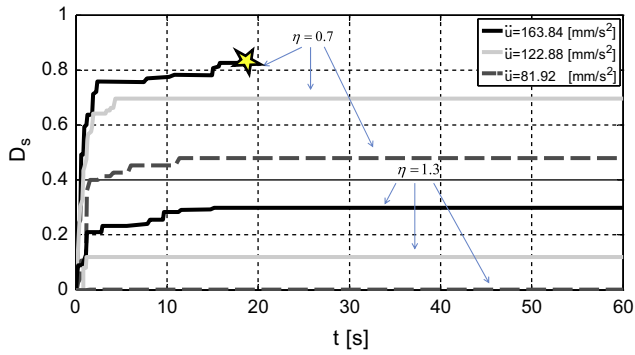


Fig. 11. Structural damage versus the time, obtained for different frequencies and different level of acceleration amplitudes of the imposed motion at the base.

of damage on the dynamic response has been analyzed through the Fourier spectral analysis. Figs. 7 and 8 show Fourier spectra of the displacement response at the time $t = 10$ s in the case of $\eta = 0.7$ and $\eta = 1.3$, respectively, for both the elastic and the proposed nonlinear damage-plastic models. Observing these figures, it can be remarked that:

- the structural system collapses before $t_f = 60$ s, for $\eta = 0.7$, when the amplitude of the imposed motion is set at $u_0 = 4$ mm;
- the development of the damage in the nonlinear model produces, away from the failure mechanism, only a decrease in time of the natural frequencies; the frequency contents become richer only when the structural system is close to the collapse condition;

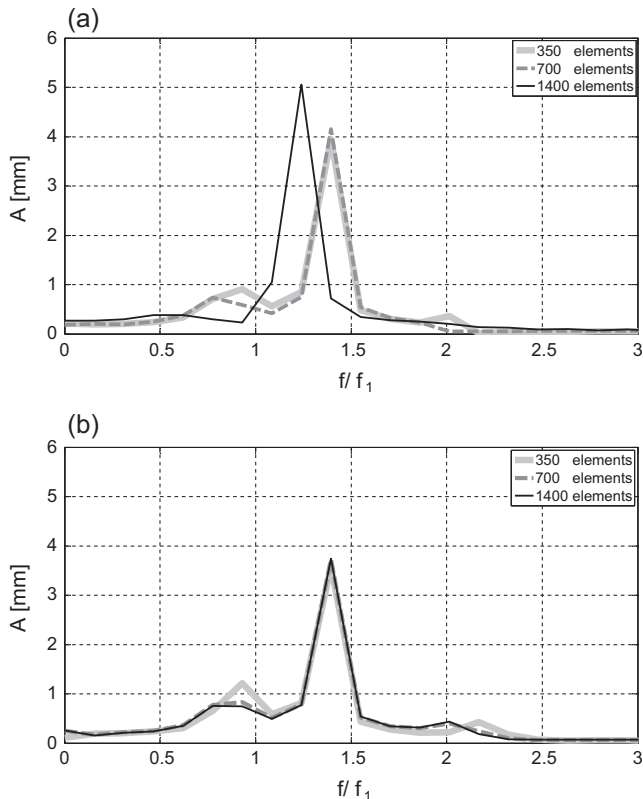


Fig. 12. Fourier spectra of the displacement response in the case $\eta = 1.3$ and $u_0 = 4$ mm for three different discretizations of the finite element modeling adopting: (a) the local damage model ($R = 0$ m); (b) the nonlocal damage model ($R = 0.4$ m).

- the reduction of the frequency contents speeds up as the forcing displacement amplitude increases.

Fig. 9 shows the time history of the displacement response for the case $\eta = 0.7$ and $u_0 = 4$ mm. Making reference to corresponding results of Fourier spectral analysis (Fig. 7c), a peculiar phenomenon can be observed. In particular, the first natural frequency of the damaged system approaches that of forcing one, at an elapsed time of about 5 s, the system goes into resonance and, as a consequence, collapses. In contrast, for the other two cases, which are characterized by lower forcing displacement amplitudes, the structural system does not reach critical condition after 5 s; instead, the damage of the structure leads only to hysteretic energy dissipation.

For the applied loadings and the imposed boundary conditions the structure tends to be damaged mainly as a consequence of reaching the tensile strength limit. In Fig. 10, the tensile damage maps are depicted at the time steps equal to 1 and 10 s for all the analysis cases. It can be remarked that:

- the damage mainly occurs at the base of the structural element;
- maintaining constant η , the increase of the displacement amplitude u_0 leads to a larger spreading of damage in the thickness of the member;
- maintaining constant u_0 , the increase of the frequency ratio η influences the propagation of the damage zone along the height of the structure.

In particular, the damage zone appears larger for the higher forcing base motion to which is associated a larger imposed acceleration. Indeed, in these cases the damage tends to develop from the base upward toward the top of the octagonal pillar, affecting only a very small zone of the ogival arches. By observing Fig. 10g–n, it appears evident that the collapse of the studied structural element does not correspond to the more severe damaging distribution because, for the case $\eta = 0.7$ and $u_0 = 4$ mm, the damage involves less volume and localizes at the base of the system. In other words, the structural collapse occurs because of the failure of the masonry at the base of the column. Indeed, in this case the damage assumes unit value along the entire section.

A structural damage variable in tension is computed through the following integral:

$$D_t^S = \frac{1}{V_{d_f}} \int_{\Omega} D_t d\Omega \tag{20}$$

where V_{d_f} is the damaged volume of the structure at the final time of the analysis. High value of D_t^S indicates that the volume V_{d_f} is affected by severe tensile damages. It can be remarked that the expression of the structural damage is not able to give information neither on the spatial distribution of the damage or where it tends to be concentrated, neither on the size of V_{d_f} , but the its determination furnishes indications on the presence of partial or complete detachment of masonry in the portion of damaged volume.

Certainly, in the previously showed cases the acceleration amplitudes (i.e. $\dot{u}_0 = u_0(2\pi f_0)^2$) are different and a direct comparison at equal level of exciting force is not possible. Undoubtedly, the frequency content plays a crucial role; indeed, a forcing frequency lower than the first natural frequency induces a peculiar evolving phenomenon in which the damage produces a reduction of the first natural frequency, moving it toward the forcing frequency. This observation is more evident if the damage evolution is compared selecting an equal level of the imposed acceleration (inertia forces) for the two forcing frequencies. Specifically, Fig. 11 records the tensile damage variable versus time for six cases, three of which characterized by a scaled imposed

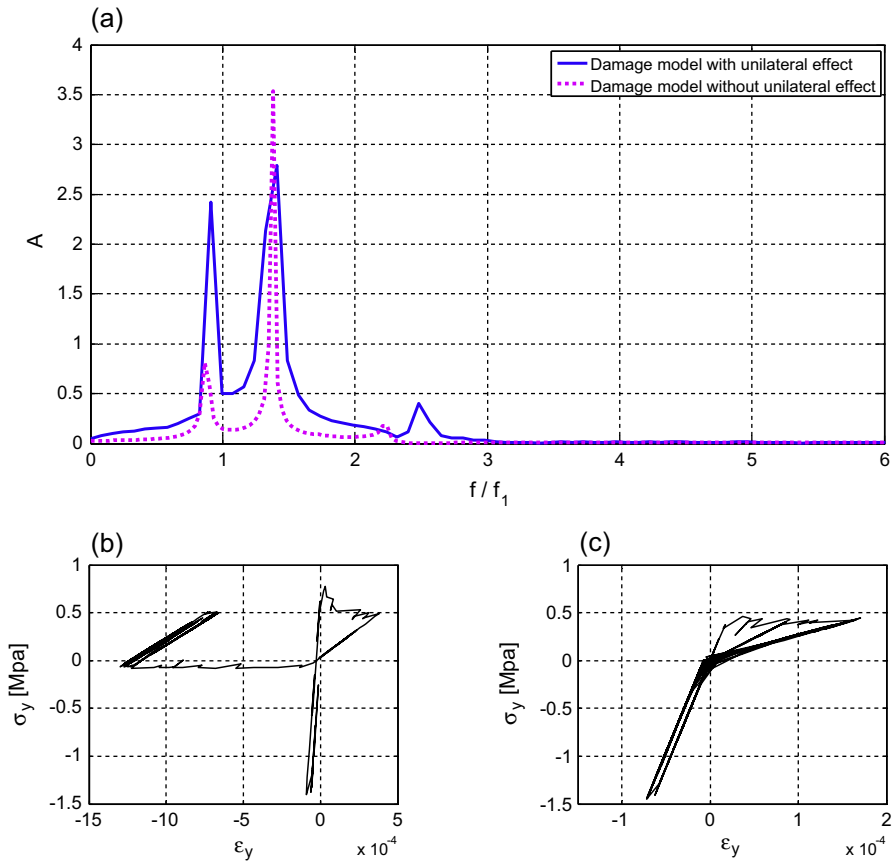


Fig. 13. (a) comparison for the case $\eta = 1.3$ and $u_0 = 4$ mm between Fourier spectra obtained by adopting a damage model without and with unilateral effect; (b) local response without the unilateral effect; (c) local response with the unilateral effect.

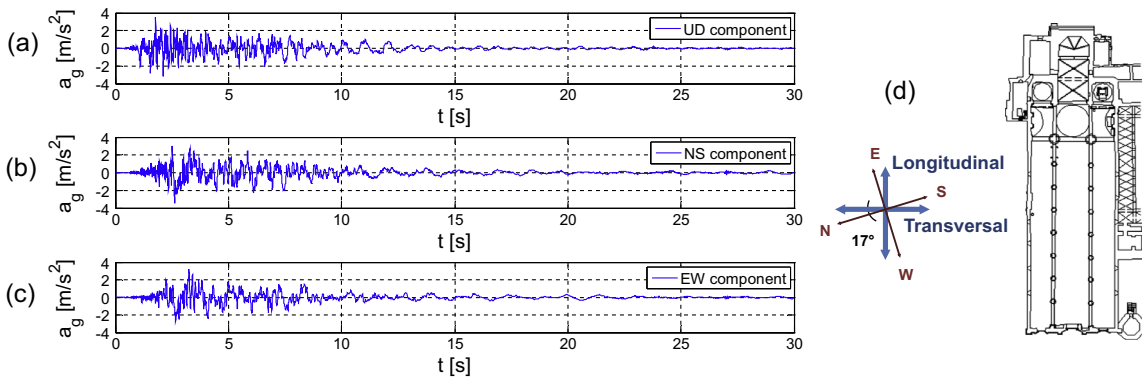


Fig. 14. Waveforms of L'Aquila earthquake: (a) UD acceleration component; (b) NS acceleration component; (c) EW acceleration component; (d) NS and EW directions with respect to the basilica.

acceleration at two different excitation frequencies. By observing Fig. 11 reached a certain level of imposed acceleration (bold black curves), the collapse occurs only when the forcing frequency is lower than the first natural one, evidencing that at the same level of exciting force, the resonance mechanism produces larger damage e consequently the final collapse. The collapse mechanism of the structural system, due to a total damage of the masonry along the entire base of the column, occurs at the time step indicated in Fig. 11 with the star symbol. In particular, in correspondence of this occurrence the analysis lost significance and it was automatically interrupted. However, from Fig. 11 it is evident that in all cases the structural damage evolution follows a similar trend: in the first time interval of about 2 s, the evolution of the structural damage is very fast, then the damage remains almost constant.

For the case $\eta = 1.3$ and $u_0 = 4$ mm, the comparison between the nonlocal and local formulation is provided. Fig. 12 shows the Fourier spectral analysis of time history of the displacement u_A by adopting the local and nonlocal approach for three different discretizations of the model: 350 elements, 700 elements and 1400 elements. It is evident that the proposed nonlocal damage model, in distinction from the local one, ensures that the numerical results are not influenced by the mesh size. Indeed, at a discretization of 700 elements, the numerical response of the mechanical system can be considered mesh independent.

Finally, the effect of the unilateral behavior modeling on the dynamic response is analyzed for the case $\eta = 1.3$ and $u_0 = 4$ mm. Fig. 13a shows the comparison of Fourier spectral analysis at the time $t = 5$ s obtained by considering two material models: the

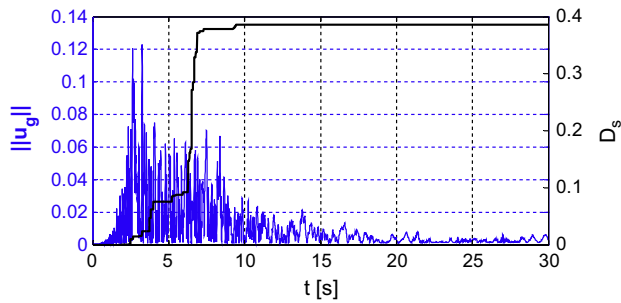


Fig. 15. Evolution of structural damage directly compared with the displacement amplitude of the L'Aquila earthquake during elapsed time.

model proposed here, which takes into account the stiffness recovery due to microcrack closure after decrease in stiffness for tensile cracking; and the same model from which this unilateral effect is removed. From the comparison of Fig. 13a, it appears clear that the unilateral phenomenon significantly influences the masonry dynamic behavior. Indeed, the model, which does not consider the unilateral phenomenon, tends to underestimate the contents of the natural frequencies of a damaging system. Fig. 13b and c illustrate the stress-strain curves obtained by assuming the damage model with the unilateral effect and without unilateral effect, respectively, at a Gauss point of the finite element located in correspondence of the left corner at the base. Note that the scale of the two plots are different. From the figures, it can be observed that: in the model without unilateral effect (Fig. 13b), both the damage in tension and the damage in compression evolve; in the model with unilateral effect (Fig. 13c) the damage in tension evolves, while the damage in compression is not activated.

4.5. 2009 L'Aquila earthquake

This section develops a damage analysis of a structural member, a central hall pillar, damaged in the 2009 L'Aquila earthquake [25].

The Up–Down (UD), North–South (NS) and East–West (EW) earthquake acceleration components are shown in Fig. 14. As can be observed in Fig. 14, the longitudinal and transversal directions of the basilica are positioned at a rotation of 17° with respect to the true NS and WE directions. In order to perform an out-of-plane analysis of the structure, the sum of the transversal components of the NS and WE accelerations, together with the UD acceleration

component, are considered. The transversal components of the NS and WE accelerations are the projections on the transversal direction of the Basilica, which is illustrated in Fig. 14.

The seismic analysis is conducted by imposing at the base of the system a motion in term of displacements obtained by performing a twice numerical time integration of the transversal acceleration components and by considering a time step equal to 0.005 s, corresponding to the acquisition frequency of the earthquake data.

The magnitude of the imposed base displacement and the tensile structural damage are plotted versus the time in Fig. 15. As regards the time evolution of the damage, three phases can be distinguished: from the beginning of the earthquake until 3 s, the damage is null; during the period of 2–9 s, the growth of damage occurs quickly; after 10 s, the structural damage remains constant. It is evident from the figure that the development of the damage is closely related to the seismic action, since precisely in the 2–9 s interval the displacement amplitude becomes more pronounced and the frequency of oscillations higher.

Tensile damage maps at significant time steps during the damage evolution phase (i.e. 2, 5, 8 and 9 s) are depicted in Fig. 16. It can be noted that: the damaging remains localized in the stone column; initially the damage occurs at the top of the column in correspondence with the connections at the ogival arch; the damage then develops at the base of the column and tends to propagate upward, involving a large part of the structural element; although the column is severely damaged at the base and top, local collapse does not occur.

Finally, a comparison between the local and nonlocal formulations in predicting the final damage propagation is provided in Fig. 17. The structural damage determined with the local model appears lower than the one defined through the use of the regularization technique. Making reference to Figs. 3b,c and 17, it can be emphasized that the nonlocal approach better simulates the final degradation of the structure than does the local model. Specifically, the nonlocal model is able to catch a diffusion and a level of the damage more realistic than the local model, by which the obtained damaging appears heavily localized and underestimated. Indeed, the damages provided by the nonlocal model appears widespread at the base and at the top of the columns, affecting a very extensive area of the structural system. Moreover, the simulated degradation really occurs in those zones where the macrocracks have been developed because of 2009 L'Aquila earthquake.

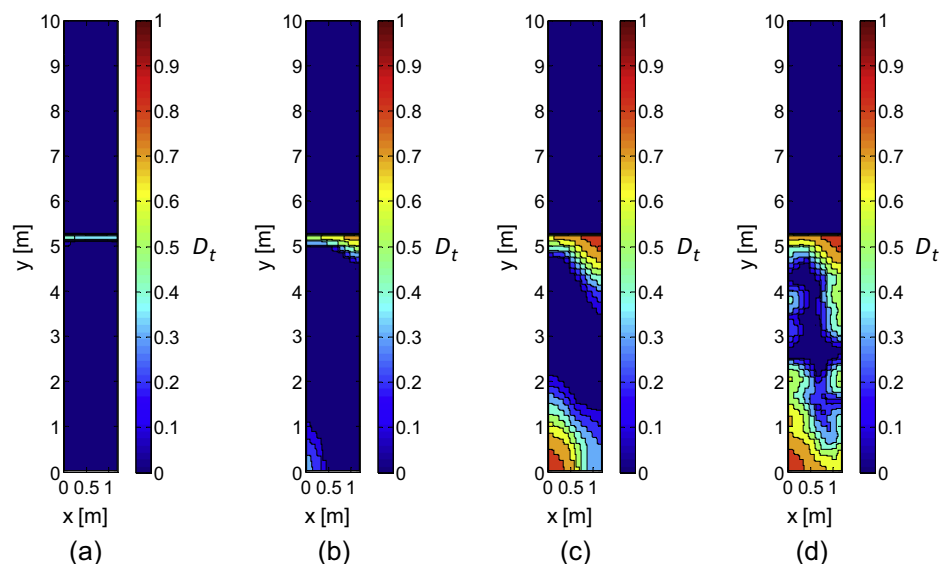


Fig. 16. Damage maps at time steps: (a) $t = 2$ s; (b) $t = 5$ s; (c) $t = 8$ s, (d) $t = 9$ s.

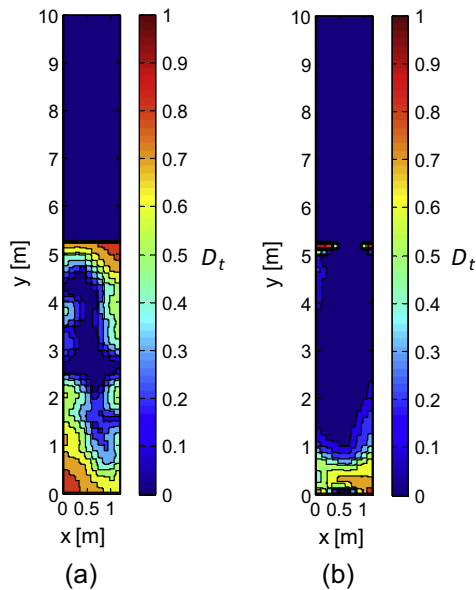


Fig. 17. Final damage map: (a) nonlocal model; (b) local model.

5. Conclusions

A nonlocal damage-plastic model is proposed and applied to the dynamic analysis of a large-scale masonry structure; the model has been used to characterize the damage propagation induced by an imposed base motion. For this purpose, two different types of motions are considered: a simple harmonic motion and the motion induced by the 2009 L'Aquila earthquake.

In the first series of direct time integrations of the discretized model, simple harmonic motions are imposed at the base in order to evidence the effect of both the amplitude and the frequency content of the base motion on the damage propagation. The analyses conducted in both the time and frequency domains show that base motion at a higher forcing frequency than the first natural one is accompanied by large accelerations and consequently by a large response, which produces a faster damage propagation; however, in the case of a forcing frequency lower than the first natural one due to the stiffness degradation, even in the presence of a small imposed acceleration, collapse occurs due to an ongoing resonance mechanism between the decreasing first natural frequency and the lower forcing frequency. The numerical examples show that the damage model is able to capture the dissipation of energy and the reduction of the natural frequency occurring in system undergoing damage.

Damage analysis caused by the 2009 L'Aquila earthquake demonstrates the efficacies and the applicability of the proposed model in predicting the final degradation state of the examined structural element. Indeed, the diffusion and the level of the damage obtained through the finite element modeling appears realistic and in agreement with the observed damage that occurred in the columns after the earthquake.

Finally, numerical applications demonstrated that the developed computational procedure is reliable for the analyses of damaging structures subjected to softening. The regularization in the constitutive law avoided strange irregularities in the structural response and allowed a smooth convergence of the iterative procedure. Moreover, numerical tests proved the advantages provided by the proposed nonlocal regularization technique over the local approach. Indeed, the independence of the numerical results from the discretization is shown in the case of sinusoidal loading. The ability of the computational tool is demonstrated for the realistic

simulation of the structural damage caused by the L'Aquila earthquake, for which the damage field numerically evaluated matches the state of damage of the examined structural element.

Acknowledgements

This research has been developed thanks to the financial support of the Italian Ministry of Education, University and Research (MIUR) through PRIN project "Dynamics, Stability and Control of flexible structures" (code 2010JK5B) and to ReLUIIS (Italian Ministry of the Civil Protection).

References

- [1] Pijaudier-Cabot G, Bažant Z. Nonlocal damage theory. *J Eng Mech* 1987;113(10):1512–33.
- [2] Borino G, Failla B, Parrinello F. A symmetric nonlocal damage theory. *Int J Solids Struct* 2003;40:3621–45.
- [3] Jirásek M, Rolshoven S. Comparison of integral-type nonlocal plasticity models for strain-softening materials. *Int J Eng Sci* 2003;41(13–14):1553–602.
- [4] Nguyen G, Korsunsky AM. Development of an approach to constitutive modelling of concrete: isotropic damage coupled with plasticity. *Int J Solids Struct* 2008;45:5483–501.
- [5] Andreus U, Casini P, Vestroni F. Nonlinear dynamics of a cracked cantilever beam under harmonic excitation. *Int J Nonlinear Mech* 2007;42:566–75.
- [6] Jassim ZA, Ali NN, Mustapha F, Abdul Jalil NA. A review on the vibration analysis for a damage occurrence of a cantilever beam. *Eng Fail Anal* 2013;31:442–61.
- [7] Zheng L, George DH. Seismic damage analysis of RC structures using fiber beam-column elements. *Soil Dyn Earthq Eng* 2012;32:103–10.
- [8] Patzák B, Rypal D, Bittnar Z. Parallel explicit finite element dynamics with nonlocal constitutive models. *Comput Struct* 2001;79:2287–97.
- [9] Voyiadjisa GZ, Abu Al-Ruba RK, Palazotto AN. Thermodynamic framework for coupling of non-local viscoplasticity and non-local anisotropic viscodamage for dynamic localization problems using gradient theory. *Int J Plasticity* 2004;20:981–1038.
- [10] Shen HS, Xu YM, Zhang CL. Prediction of nonlinear vibration of bilayer graphene sheets in thermal environments via molecular dynamics simulations and nonlocal elasticity. *Comput Methods Appl Mech Eng* 2013;267:458–70.
- [11] Ahad FR, Enakoutska K, Solanki KN, Bammann DJ. Nonlocal modeling in high-velocity impact failure of 6061-T6 aluminum. *Int J Plasticity* 2014;55:108–32.
- [12] Welemane H, Goidescu C. Isotropic brittle damage and unilateral effect Endommagement isotrope fragile et effet unilatéral. *CR Mécanique* 2010;338:271–6.
- [13] Zhua QZ, Shaoa JF, Kondoa D. A micromechanics-based thermodynamic formulation of isotropic damage with unilateral and friction effects. *Eur J Mech A – Solid* 2010;30:316–25.
- [14] Lanoyea E, Cormerya F, Kondob D, Shao JF. An isotropic unilateral damage model coupled with frictional sliding for quasi-brittle materials. *Mech Res Commun* 2013;53:31–5.
- [15] Toti J, Marfia S, Sacco E. Coupled body interface nonlocal damage model for FRP detachment. *Comput Methods Appl Mech* 2013;260:1–23.
- [16] Zienkiewicz OC, Taylor RL. *The finite element method*. 4th ed. London: McGraw-Hill; 1991.
- [17] Taylor RL. FEAP-A finite element analysis program, Version 8.3. Department of Civil and Environmental Engineering, University of California at Berkeley, California; 2011.
- [18] Antonacci E, Beolchini GC, Di Fabio F, Gattulli V. The dynamic behaviour of the basilica S. Maria di Collemaggio. In: Proc. of 2nd international congress on studies in ancient structures. Instabul (Turkey); 9–13 July 2001.
- [19] Federici F, Graziosi F, Faccio M, Gattulli V, Lepidi M, Potenza F. An integrated approach to the design of Wireless Sensor Networks for structural health monitoring. *Int J Distrib Sens Netw* 2012;2012:16.
- [20] Gattulli V, Graziosi F, Federici F, Potenza F, Colarieti A, Lepidi M. Structural health monitoring of the basilica S. Maria di Collemaggio. Research and Applications in Structural Engineering, Mechanics and Computation Edited by Alphonse Zingoni. 2013, p. 2291–6 [chapter 382].
- [21] Gattulli V, Antonacci E, Vestroni F. Field observations and failure analysis of the Basilica S. Maria di Collemaggio after the 2009 L'Aquila earthquake. *Eng Fail Anal* 2013;34:715–34.
- [22] Pastor M, Binda M. Modal assurance criterion. *Model Mech Mech Syst* 2012;48:543–8.
- [23] Foti D, Gattulli V, Potenza F. Output-only identification and model updating by dynamic testing in unfavorable conditions of a seismically damaged building. *Comput – Aided Civil Infrastruct Eng* 2014;29(9):659–75.
- [24] MATLAB R2010a, Natick (Massachusetts, United States): The MathWorks Inc.
- [25] Ceci AM, Contento A, Fanale L, Galeota D, Gattulli V, Lepidi M, Potenza F. Structural performance of the historic and modern buildings of the University of L'Aquila during the seismic events of April 2009. *Eng Struct* 2010;32(7):1899–924.